Quantifying the role of N-position in Imine based Covalent Organic Frameworks for Photocatalytic Water Splitting

Palak Chugh, Arup Mahata*

Department of Chemistry, Indian Institute of Technology Hyderabad, Kandi, Sangareddy 502284, India

E-mail: arup@chy.iith.ac.in

Supporting information

Text S1: Computational Details:

All calculations in this work have been performed using the Vienna ab initio Simulation Package (VASP), based on Density functional theory.[1,2] The exchange-correlation energy calculations have been described using the generalized gradient approximation (GGA) with the Perdew-Burke-Ernzerhof (PBE) functional.[3] Core electron interactions have been defined using the projector augmented wave (PAW) pseudopotential.[4] To account for long-range van der Waals interactions, Grimme's D3 dispersion correction (DFT-D3) has been applied.[5] To describe the plane wave basis set energy cutoff is set to be 470 eV. To avoid the interaction between the layers vacuum of 15Å is employed in the z direction. Brillouin zones have been sampled using a Γ-centered 2×2×1 k-points mesh. The convergence criteria for energy and force have been set at 10^{-4} eV and 0.01 eV/Å, respectively. As the PBE functional underestimates electronic properties, hybrid functional calculations have been employed for more accurate electronic structure and band alignment analysis. Furthermore, the G_0W_0 method has been employed to calculate the quasiparticle band gap, and it has been combined with the Bethe–Salpeter equation (BSE) to evaluate the optical band gap and exciton binding energy. The computational hydrogen electrode (CHE) model has been used to calculate the free energy (ΔG) for the hydrogen evolution reaction (HER) and oxygen evolution reaction (OER) processes developed by Nørskov et al. [6] Post-analysis have been performed using VASPKIT[7] and VESTA.[8]

Formation Energy:

The formation energy of all designed COFs is carried out according to the following general formula:

$$E_f = \frac{E(AmBn) - mE(A) - nE(B)}{m+n}$$

where E is the total energy of the structural unit cell, E(A) and E(B) are the single atomic energy of the constituent elements in the reference state, and m and n are the number of atoms of the corresponding elements in the unit cell.[9,10]

Free Energy:

The thermodynamics of water splitting is evaluated by examining the free energy changes associated with the hydrogen evolution reaction (HER) and oxygen evolution reaction (OER). The reactions involved in HER and OER were described by elementary steps.

HER is two electron step reaction, the first step involves the adsorption of a proton onto the catalyst surface, forming an adsorbed hydrogen intermediate (H), while the second step involves the reduction of this intermediate via electron transfer, releasing molecular hydrogen (H_2).

Step1:

$$* + H^+ + e^- = {}^*H$$

Step2:

$${}^*H + H^+ + e^- = * + H_2$$

OER is four electron steps consisting of four elementary steps:

Step 1:

$$* + H_2O = *H\text{-}OH$$

Step 2:

$$*H\text{-}OH = *H\text{-}O + H^+ + e^-$$

Step 3:

$$*H\text{-}O + H_2O = *H\text{-}OOH + H^+ + e^-$$

Step 4:

$$*H\text{-}OOH = * + O_2 + 2(H^+ + e^-)$$

Here, * denotes a site on the surface, and *(radical) denotes the corresponding radical adsorbed on the surface.

The empirical Brønsted–Evans–Polanyi (BEP) relationship describes a linear dependence between the activation barrier of an elementary reaction step and its corresponding reaction energy. This correlation provides a mechanistic basis for estimating kinetic behavior from thermodynamic descriptors, allowing reaction barriers to be inferred without explicit performing transition-state calculations.[11–13] Gibbs free energy change (ΔG) for each step has been computed using the computational hydrogen electrode (CHE) model by Nørskov et. al. Gibbs free energy (ΔG) is defined as

$$\Delta G = \Delta E + \Delta E_{ZPE} - T\Delta S + \Delta G_U + \Delta G_{pH}$$

Here, ΔE is the reaction energy calculated from DFT calculations. ΔE_{ZPE} is the zero-point energy, T is the system temperature (298.15 K), and ΔS is the entropy change. ΔG_U refers to the extra potential bias provided by an electron in the electrode, where U is the electrode potential relative to the NHE. For HER, potential provided through photogenerated electrons (U_{red}) is defined as the energy difference between the hydrogen reduction potential and the conduction band minimum (CBM). For OER, the potential provided through photogenerated holes (U_{ox}) are defined as the energy differences between the valence band maximum (VBM) and the hydrogen reduction potential.

The thermodynamic performance of HER and OER can be seen by estimating the overpotential of the reaction (η), which is calculated by:

$\eta_{HER} = \max \{\Delta G_1, \Delta G_2\}/e$

η_{OER} = max $\{\Delta G_3, \Delta G_4, \Delta G_5, \Delta G_6, \Delta G_7\}$/e -1.23

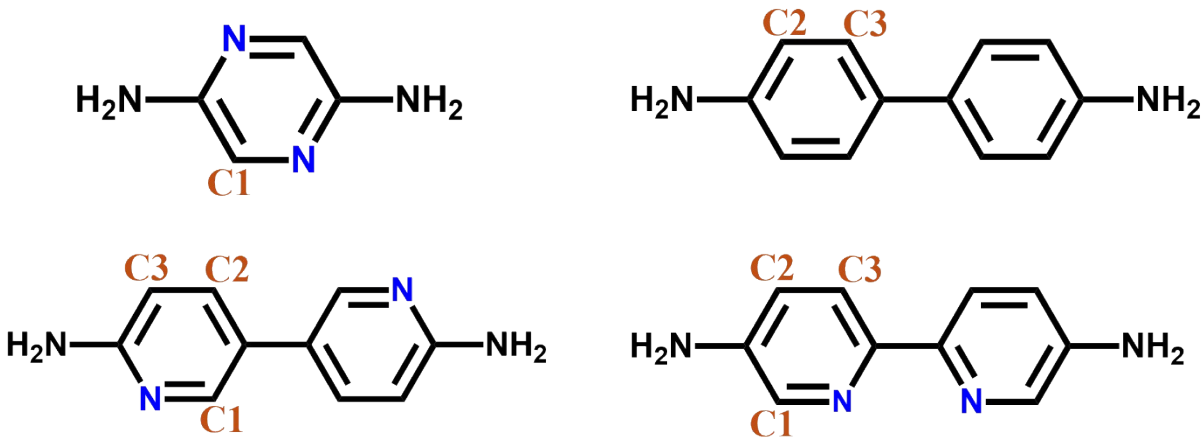

Figure S1. Illustration of potential OER-active sites in the COF structure.

Text S2: Thermodynamic Pathway Selectivity for OER in COFs.

OER constitutes the rate-limiting half-reaction in water splitting due to its intrinsically high thermodynamic and kinetic barriers and the involvement of multiple proton-electron transfer steps. Depending on the reaction energetics, water oxidation may follow a 1e, 2e, or the desired 4e pathway, generating $OH\cdot$, H_2O_2, or O_2, respectively. To elucidate the pathway selectivity of the investigated COFs, we performed a thermodynamic analysis of the adsorption free energies of OH* (ΔG_{OH*}) and O* (ΔG_{O*}) at the catalytically active more probable site (C1S), proposed by Nørskov et al. [14] Using these adsorption energies, we constructed a thermodynamic selectivity map that differentiates between the 1e, 2e, and 4e oxidation domains, thereby allowing prediction of the predominant water oxidation route for each COF (Figure S3). All studied COFs exhibit ΔG_{OH*} values below 2.38 eV and ΔG_{O*} values below 3.52 eV, unequivocally placing them within the 4e oxidation regime. Such energetics indicate that the adsorbed OH* species spontaneously progress to O* and further evolve into O_2, rather than terminating at the 2e pathway producing H_2O_2. This thermodynamic preference highlights the intrinsic tendency of these COFs to drive the full four-electron OER mechanism. Based on these insights, the catalytic surface activity and OER performance of the COFs are examined in the subsequent section.

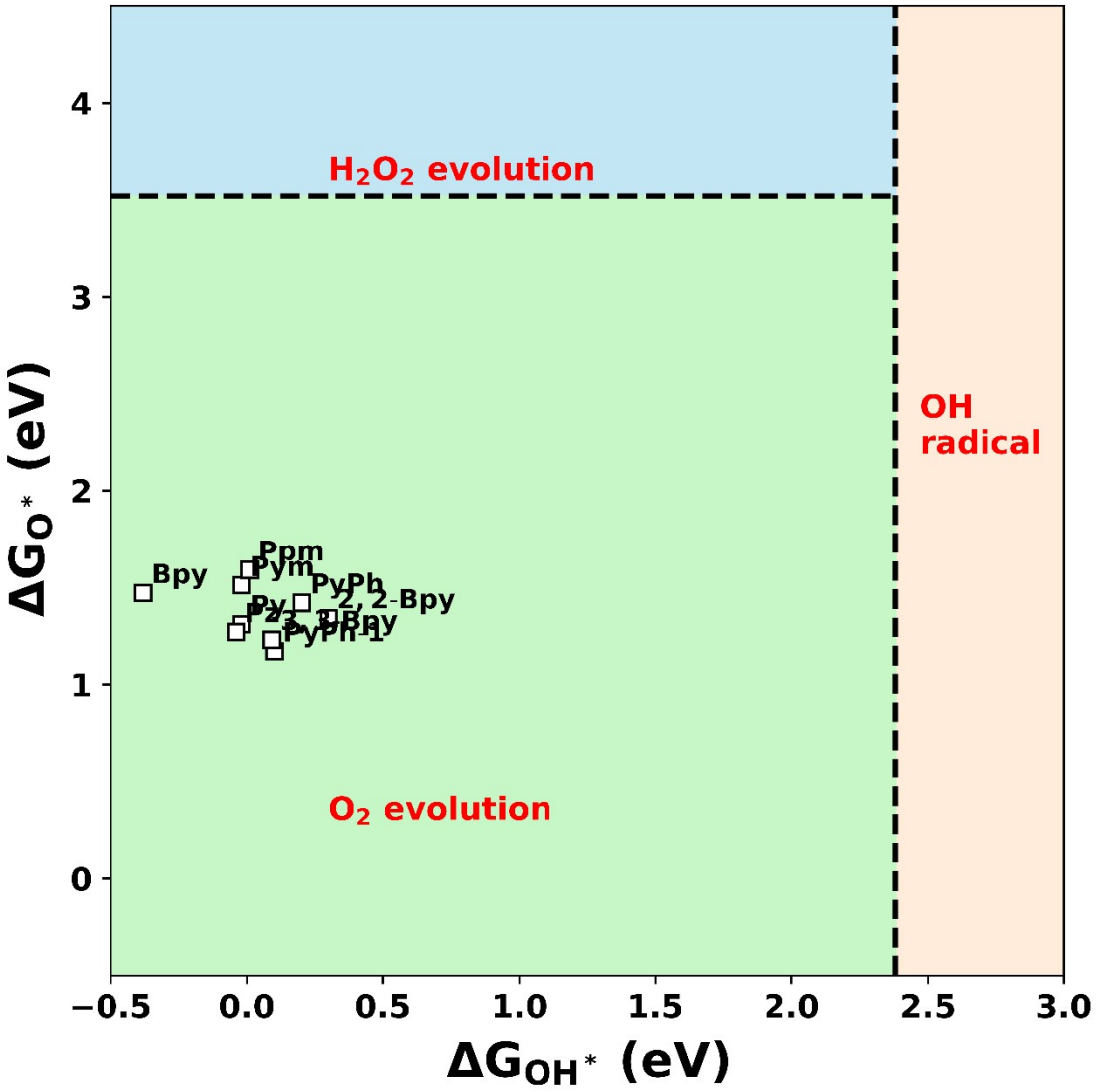

Figure S2. Selectivity map among possible water oxidation pathways (OH·, H_2O_2, O_2) based on thermodynamic adsorption energies of ΔG_{OH*} and ΔG_{O*} for all studied COFs at C1S site with pH = 7. The dotted lines represent critical thresholds: ΔG_{OH*} = 2.38 eV and ΔG_{O*} = 3.52 eV. Catalysts located in the green region favor the $4e^-$ OER (O_2 evolution).

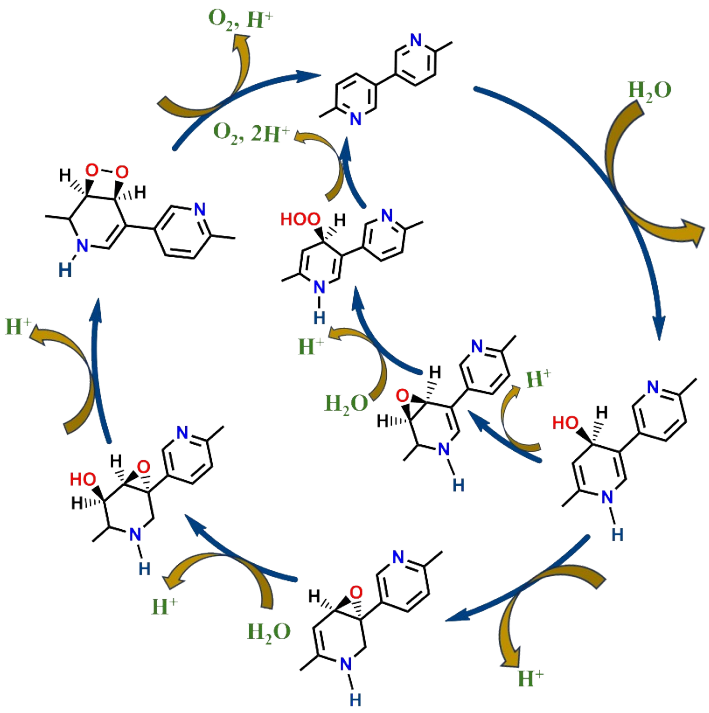

Figure S3. Proposed water oxidation pathways on 3,3-Bpy, illustrating two possible pathways, single-site and dual-site.

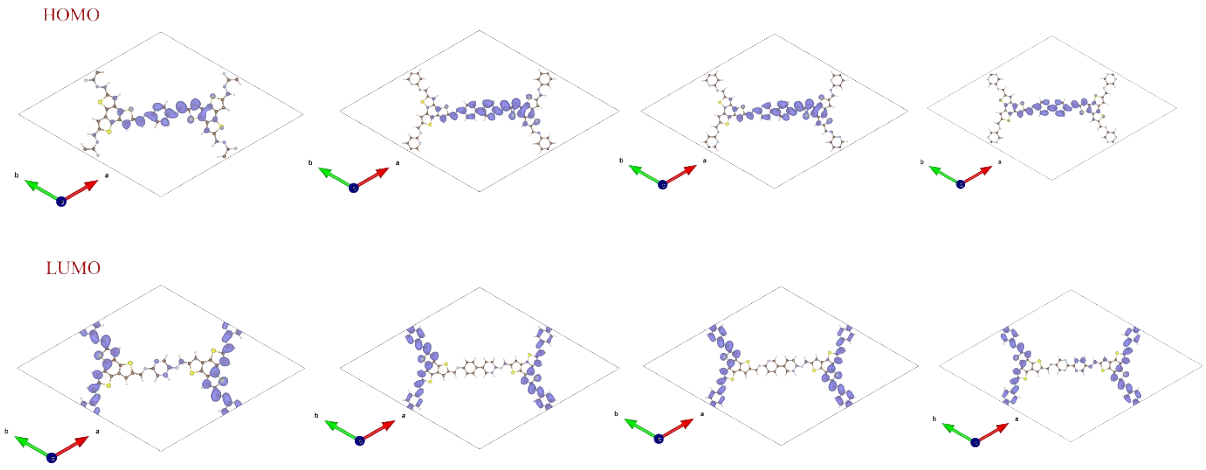

Figure S4. HOMO and LUMO electron cloud distribution on protonated **a)** Pz **b)** PyPh-1 **c)** 3,3-Bpy **d)** Bpym COFs

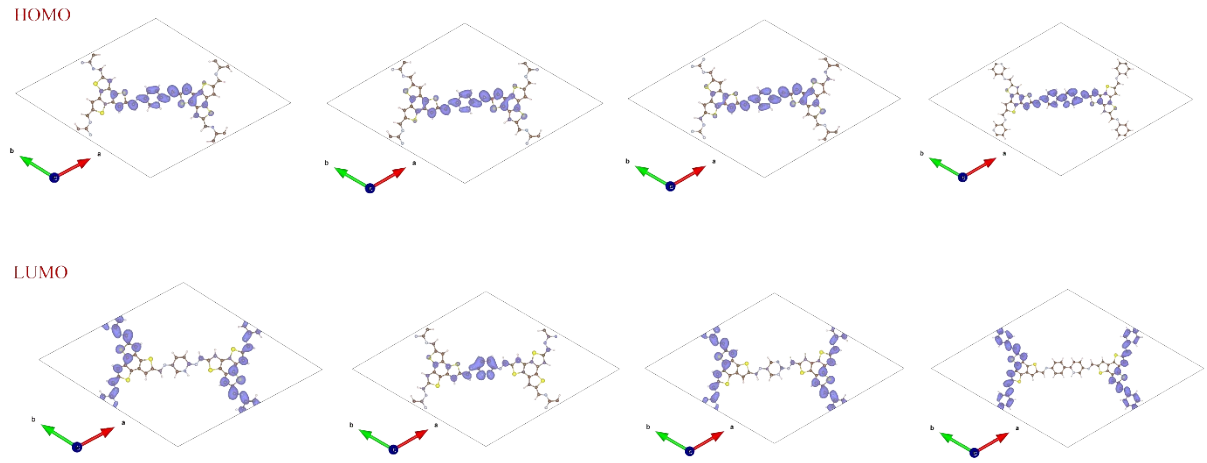

Figure S5. HOMO and LUMO electron cloud distribution on protonated **a)** Py **b)** Pzd **c)** Pym **d)** PyPh COFs

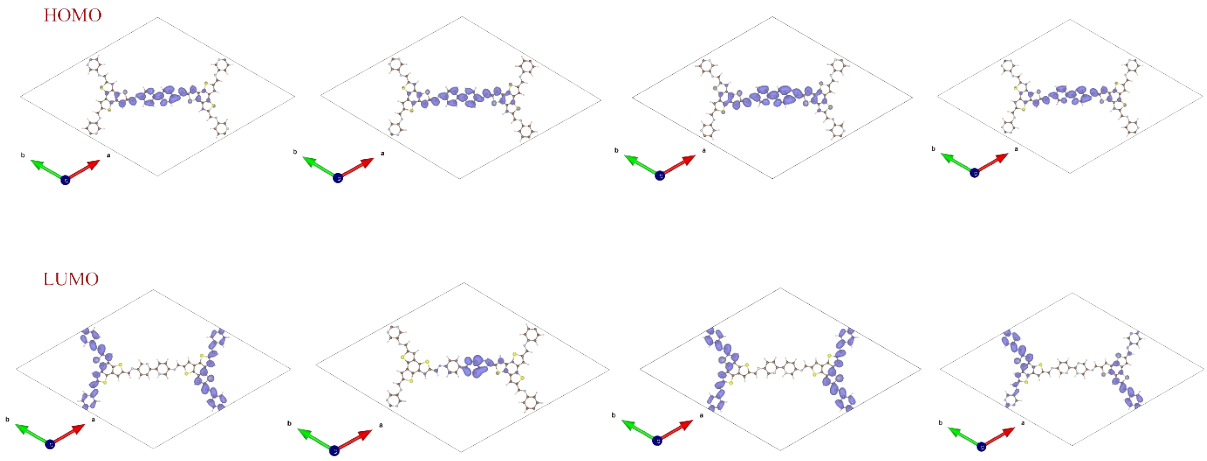

Figure S6. HOMO and LUMO electron cloud distribution on protonated **a)** 2,2-Bpy **b)** Ppm **c)** Bpy **d)** Pym-Py COFs

Text S3: Frontier Orbital of COFs

HOMO–LUMO of the pristine COFs for each type shown in Scheme 1 is shown Figure S4. As one can see that, in this pristine state, both HOMO and LUMO orbitals are delocalized across the COF framework; specifically, the HOMO is primarily contributed by the BTT units, while the LUMO is mainly localized on the bipyridine based linkers. These results confirm that the intrinsic COF architecture indeed follows the designed donor–acceptor electronic structure.

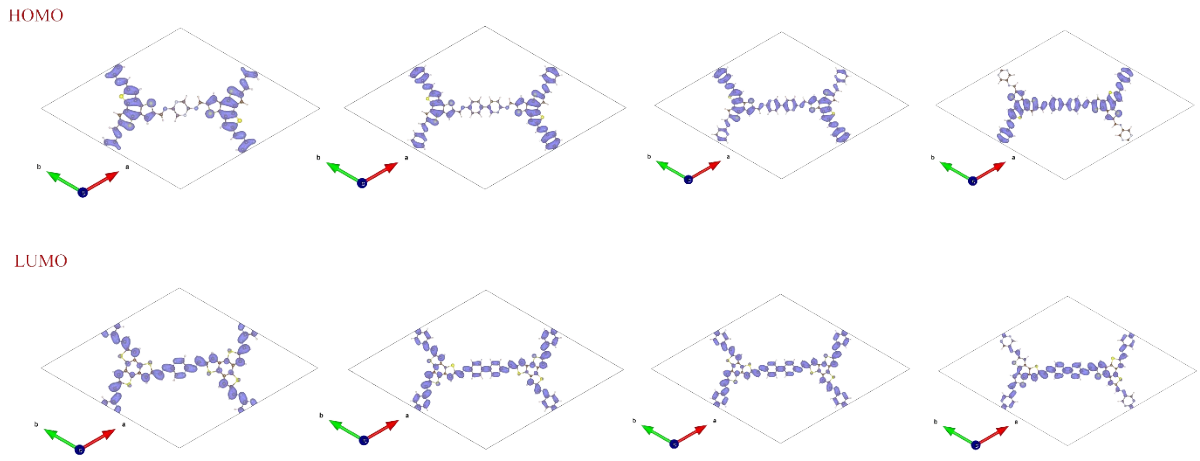

Figure S7. HOMO and LUMO electron cloud distribution on pristine a) Pz b) PyPh-1 c) 3,3-Bpy d) Bpym COFs

Table S1. lattice constants (Å) for 2D-COFs.

COF	a=b/ Å
Ph	28.58
BPH	36.53
Bpy	36.30

Table S2. Formation energies (eV) for 2D-COFs.

COF	E_f/eV
Ph	-0.45
Py	-0.76
Pzd	-1.07
Pym	-1.10
Pz	-1.09
BPH	-0.33
PyPh	-0.55
PyPh-1	-0.54
2,2-Bpy	-0.79
3,3-Bpy	-0.77
Ppm	-0.79
Bpy	-0.78
Pym-Ph	-1.03

Bpym	-1.28

Table S3. Bader charge Analysis of all COFs and COFs-H.

COF	**Before Protonation**		**After Protonation**	
	Charge on N (e)	**Charge on ortho C (e)**	**Charge on N (e)**	**Charge on ortho C (e)**
Py	-1.06	0.43	-1.28	0.33
Pym	-1.18	0.60	-1.29	0.44
Pz	-1.19	0.56	-1.26	0.33
PyPh	-1.25	0.64	-1.29	0.42
PyPh-1	-1.15	0.62	-1.21	0.33
2,2-Bpy	-1.23	0.50	-1.26	0.39
Ppm	-1.25	0.48	-1.33	0.36
Bpy	-1.17	0.53	-1.33	0.41
Py-Pym	-1.18	0.56	-1.32	0.48
BPym	-1.17	0.46	-1.23	0.39

Table S4. Limiting potential of OER and HER of designed COFs.

COF	Limiting Potential OER (V)				Limiting Potential HER (V)
	C1S	C2S	C2D	C3S	
Ph	-	2.57	1.74	-	0.86
Py	1.31	1.55	1.78	1.85	0.06
Pzd	-	1.64	2.55	-	0.04
Pym	1.51	-	-	-	-0.01
BPH	-	2.39	1.59	2.41	0.64
PyPh	1.42	1.67	2.26	1.77	0.41
2,2-Bpy	1.34	1.45	1.98	1.77	0.41
Ppm	1.59	-	-	-	0.26
Bpy	1.34	1.55	1.78	1.86	0.34
Py-Pym	1.33	-	-	-	0.31

Table S5. Adsorption energies (ΔG) for OER intermediates along Pathway C1S and HER at pH=7.

COF	ΔG_{OH*}	ΔG_{O*}	ΔG_{OOH*}	ΔG_{H*}
Py	-0.02	1.31	1.16	0.06
Pym	-0.20	1.51	0.98	-0.01
Pz	-0.04	1.27	1.19	0.02
PyPh	0.20	1.42	0.95	0.42
PyPh-1	0.10	1.17	1.28	-0.04
2,2-Bpy	0.30	1.34	1.11	0.41
3,3-Bpy	0.09	1.23	1.25	0.02
Ppm	0.01	1.59	0.87	0.26
Bpy	-0.34	1.34	1.07	0.34
Py-Pym	-0.21	1.33	1.13	0.31
Bpym	-0.38	1.47	1.03	0.28

Table S6. The driving potentials of photogenerated electrons (U_{red}) and holes (U_{ox}) are calculated based on the band alignment of the respective COFs.

COF	U_{ox} (V)	U_{red} (V)
Ph	1.70	0.87
Py	1.41	0.71
Pzd	1.69	0.52
Pym	1.89	0.27
Pz	1.67	0.44
BPH	1.58	0.68
PyPh	1.75	0.50
PyPh-1	1.70	0.58
2,2-Bpy	1.54	0.72
3,3-Bpy	1.57	0.71
Ppm	1.54	0.72
Bpy	1.56	0.73
Py-Pym	1.73	0.59
BPym	1.92	0.47

Table S7. Bader charges distribution and their limiting potential on respective COFs.

COF	Charge on N (e)	Charge on Ortho-C (e)	Limiting Potential (V)
PyPh	-1.29	0.42	1.42
PyPh-1	-1.21	0.33	1.28
2,2-Bpy	-1.26	0.39	1.34
3,3-Bpy	-1.20	0.28	1.25

Table S8. Exciton Binding Energy (E_b) of the Investigated COFs.

COF	Fundamental Bandgap (eV)	Optical Bandgap (eV)	Exciton Binding Energy (eV)
PyPh	2.56	1.81	0.75
PyPh-1	2.52	1.83	0.69
2,2-Bpy	2.58	1.90	0.68
3,3-Bpy	2.58	1.98	0.61

References

1 G. Kresse and J. Furthmüller, *Computational Materials Science*, 1996, **6**, 15–50.

2 G. Kresse and J. Furthmüller, *Phys. Rev. B*, 1996, **54**, 11169–11186.

3 J. P. Perdew, K. Burke and M. Ernzerhof, *Phys. Rev. Lett.*, 1996, **77**, 3865–3868.

4 P. E. Blöchl, *Phys. Rev. B*, 1994, **50**, 17953–17979.

5 S. Grimme, J. Antony, S. Ehrlich and H. Krieg, *J. Chem. Phys.*, 2010, **132**, 154104.

6 E. Skúlason, G. S. Karlberg, J. Rossmeisl, T. Bligaard, J. Greeley, H. Jónsson and J. K. Nørskov, *Phys. Chem. Chem. Phys.*, 2007, **9**, 3241–3250.

7 V. Wang, N. Xu, J. C. Liu, G. Tang and W.-T. Geng, *Computer Physics Communications*, 2021, **267**, 108033.

8 K. Momma and F. Izumi, *J Appl Cryst*, 2011, **44**, 1272–1276.

9 Y.-W. Yang, H.-D. Ren, H.-Y. Zhang, Y.-N. Zhao, H.-Q. Tan and Z.-L. Lang, *ACS Appl. Mater. Interfaces*, 2025, **17**, 5038–5046.

10 F. D. Murnaghan, *Proceedings of the National Academy of Sciences*, 1944, **30**, 244–247.

11 J. N. Bronsted, *Chem. Rev.*, 1928, **5**, 231–338.

12 M. G. Evans and M. Polanyi, *Trans. Faraday Soc.*, 1938, **34**, 11–24.

13 Y. Jing, Z. Zhou, W. Geng, X. Zhu and T. Heine, Adv. Mater., 2021, **33**, 2008645.

14 S. Siahrostami, G.-L. Li, V. Viswanathan and J. K. Nørskov, *J. Phys. Chem. Lett.*, 2017, **8**, 1157–1160.